Hydrobiologia (2013) 702:171–190
DOI 10.1007/s10750-012-1319-2

PRIMARY RESEARCH PAPER

Spatial and temporal variability of light attenuation in large rivers of the Amazon

M. P. F. Costa · E. M. L. M. Novo · K. H. Telmer

Received: 28 October 2011 / Revised: 24 August 2012 / Accepted: 10 September 2012 / Published online: 5 October 2012

Abstract The light field and its relationship with biogeochemical variables were investigated in the Solimões, Negro, Amazon, Madeira, Uatumã, Trombetas, and Tapajós Rivers. In high suspended sediment rivers, total suspended matter is the primary control on light attenuation ($r = 0.8$), with colored dissolved organic matter (CDOM) being secondary ($r = -0.6$) due to scattering and absorption, respectively. Photosynthetically active radiation was the lowest (<100.0 μmol m^{-2} s^{-1} at the depth of half $Z_{1\%}$) and was limited to depths of less than 1.0 m and confined to red light. In low suspended sediment rivers, CDOM is the primary control on light attenuation ($r = 0.9$). The concentrations of chlorophyll *a* (Chla) and CDOM cause variations among these rivers. High CDOM rivers, Negro and Uatumã, are depleted (<0.5% of incoming irradiance) of blue and green light at the depth of half $Z_{1\%}$. The light spectra of low CDOM and higher Chla waters, such as the Tapajós, Uatumã, and Trombetas Rivers at rising water stage, are restricted to green and red wavelengths, and marked by high absorption at 620 and 670 nm, due to the presence of Cyanophyceae.

Keywords Light attenuation · Underwater irradiance · Phytoplankton · Sediment · Dissolved organic matter · Rivers · Amazon

Handling editor: John M. Melack

M. P. F. Costa (✉)
Department of Geography, University of Victoria, P.O. Box 3050, Victoria, BC, Canada
e-mail: maycira@uvic.ca

E. M. L. M. Novo
Instituto Nacional de Pesquisas Espaciais, São Paulo, Brazil

K. H. Telmer
School of Earth and Ocean Sciences, University of Victoria, Victoria, BC, Canada

Introduction

In the Amazon, the rainfall, geology, soil, and vegetation, as well as the physical and biogeochemical processes occurring in the catchments, produce waters with different concentrations of particulate and dissolved compounds, generally characterizing the water bodies as white, black, or clear waters. Waters with high concentrations of inorganic particulates have a major portion of their drainage area in the Andes Cordillera, where physical and chemical processes are intense. Black water rivers drain from Precambrian shields, which are characterized by permeable podsol soils, thus resulting in large quantities of dissolved organic matter in the rivers. Clear waters drain weathered shields characterized by thick clay-rich latosol soils, resulting in water that is low in dissolved matter and suspended solids, and is nutrient poor (Devol & Hedges, 2001). In fact, many of the

Amazon's rivers are a mixture of these three water types (Walker, 1990).

Conversion of forest to agriculture (Thomas et al., 2004) and conversion of forest and floodplains to mining operations (Roland & Esteves, 1998; Mol & Ouboter, 2003; Telmer et al., 2006), however, have resulted in an increase in both physical and chemical erosion, leading to higher concentrations of particulate and dissolved compounds in Amazonian waters. For example, streams flowing through areas that have changed from forest to pasture or agricultural land have higher concentrations of total suspended particulate and dissolved compounds than streams flowing through natural forested areas (Thomas et al., 2004). Mining activities have increased suspended particulate concentrations as much as 50 mg l^{-1} since 1979, when bauxite tailings were first discharged into the originally clear waters of the Batata Lake, in the watershed of the Trombetas River (Bozelli & Garrido, 2000). This has resulted in decreasing phytoplankton abundance due to light limitation (Guenther & Bozelli, 2004a) and possibly also due to algae-clay aggregation (Guenther & Bozelli, 2004b). Since the beginning of the gold rush in the 1970s, the Creporí River, in the Tapajós watershed, has changed from clear waters with suspended solids of approximately 7 mg l^{-1} to highly turbid waters with concentrations of about 500 mg l^{-1} (Telmer et al., 2006). In Suriname, mining has resulted in increased concentrations of suspended particulates up to 2,468 mg l^{-1} in disturbed streams compared with approximately 30 mg l^{-1} in undisturbed streams (Mol & Ouboter, 2003). In French Guiana, small-scale gold mining activities have caused changes in both the taxonomic and functional structure of diatoms assemblage as a function of increased water turbidity (Tudesque et al., 2012).

Changes in the light field of Amazonian waters occur due to changes in particulate and dissolved matter caused by the different characteristics of the rivers' sub-basins, the biogeochemical processes, the mixing of different types of water, the hydrology, and human activities. However, these changes have been reported mainly for lakes, and focussed on light integrated in the photosynthetically active radiation (PAR) spectrum (Furch et al., 1985; Roland & Esteves, 1998; Melack & Forsberg, 2001; Guenther & Bozelli, 2004a). From these studies, PAR has been shown to limit phytoplankton primary production in Amazonian lakes under low human impacts (Melack & Forsberg, 2001), lakes affected by gold mining (Mol & Ouboter, 2003), and lakes affected by bauxite mining (Roland & Esteves, 1998; Guenther & Bozelli, 2004a).

PAR is attenuated at different rates in different regions of the spectra for different types of waters, and is important for understanding phytoplankton abundance and distribution (Kirk, 1994; Arst et al., 2000); therefore, it is important to spectrally resolve the vertical attenuation coefficient and the underwater irradiance for different Amazonian waters. Although the general description of in-water PAR for some Amazonian lakes has already been documented, there is a gap in knowledge about the characteristics of the spectral light field and associated water optical constituents in large rivers of the Amazon basin. The objective of this study was to investigate the spectral light field and its relationship to the optical water constituents in the Amazon River and six of its largest tributaries at two stages of the hydrological cycle, receding and rising waters. In order to accomplish this, we quantified the relationship between spectral downwelling attenuation coefficient, $K_{d(\lambda)}$, and in situ measured biogeochemical variables, total suspended solids (TSS), chlorophyll *a* (Chla), and absorption by dissolved organic matter ($a_{CDOM(440)}$). We further analyzed the measured normalized downwelling irradiance, $E'_{d(z,\lambda)}$, and quantum irradiance over the PAR range, $q_{d(PAR,z)}$, from just below the water surface down to a depth at which PAR declined to 1% ($Z_{1\%}$). This research presents the first detailed investigation of the in-water light field and its relationship to biogeochemical variables and the hydrology of large Amazonian rivers, thus adding to our understanding of Amazonian water optics and related biogeochemical variables.

Methods

Study area

Seven of the major tributaries of the Amazon River and several stretches of the Amazon River were sampled (Fig. 1). We conducted sampling along an 800 km reach of the Amazon River, beginning upstream from the Solimões and Negro confluence, ending at the Tapajós River at Santarém. Samples

were collected generally in the onset of the receding waters (2005) and onset of the rising waters (2006) in the following rivers: Solimões, Negro, Amazon (three to four different stretches of the river), Madeira, Uatumã, Trombetas, and Tapajós. The Amazon mainstem samples were from locations downstream of the confluences of the Negro/Solimões, Madeira, Uatumã, and Tapajós Rivers. The tributary samples were taken well upstream of confluences to avoid any influence of the Amazon River.

General characteristics of the sampled rivers

The Solimões, Amazon, and Madeira Rivers originate in the Andean Cordillera. Due to high relief, high precipitation, and geology characterized by sedimentary and metamorphic rocks, the Andean region is characterized by high erosion rates, resulting in high concentrations of suspended unweathered minerals, clays, and dissolved ions in the rivers. These rivers are, therefore, characterized as rich in nutrients, tend to

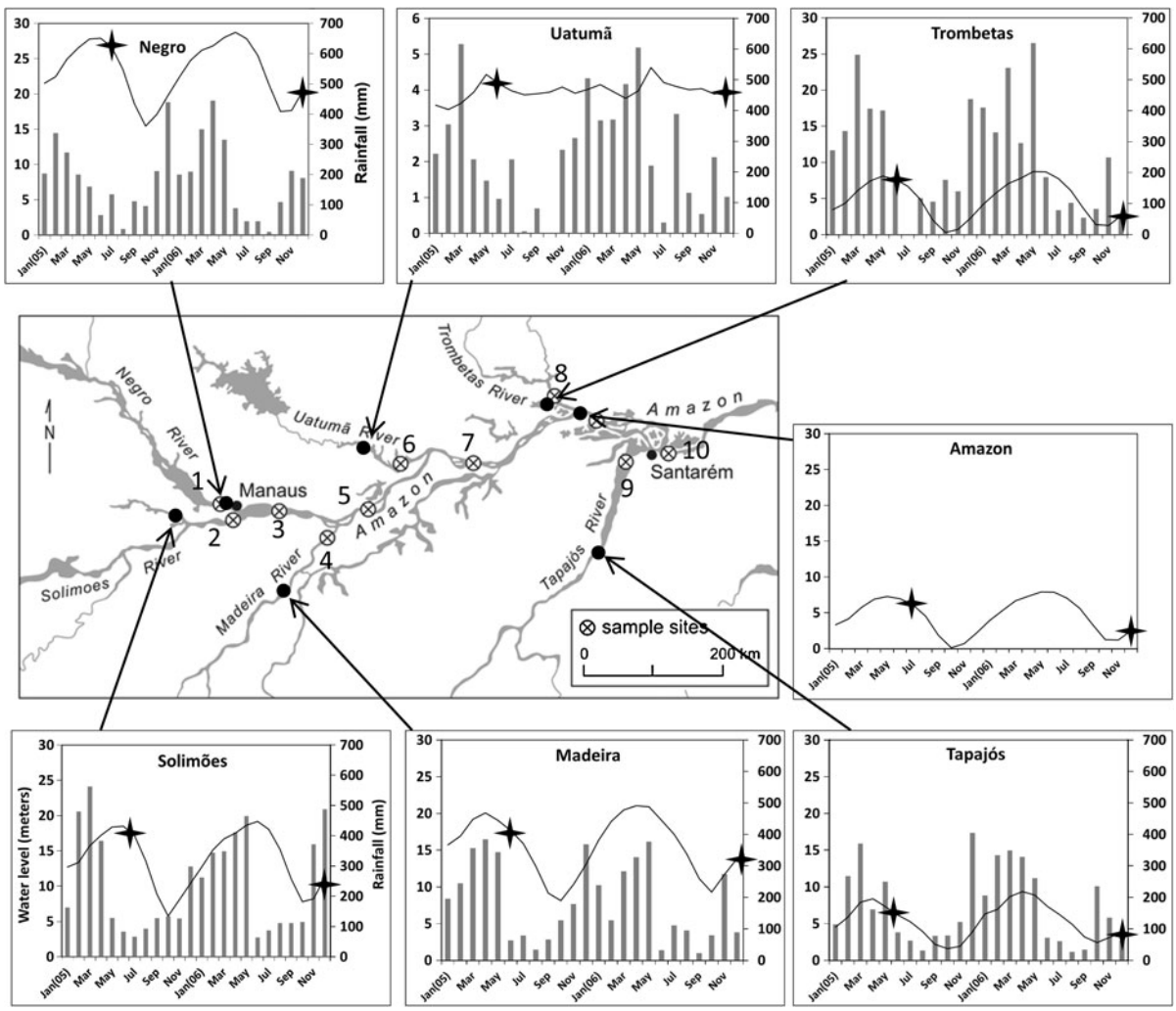

Fig. 1 Sampling locations on the Amazon River and its major tributaries with their respective water level (*continuous line*) and rainfall (*bars*) for the years 2005 and 2006. Mainstem sampling locations are called Amazon 1 (3), Amazon 2 (5), Amazon 3 (7), and Amazon 4 (10). Other sampled rivers are Negro (1), Solimões (2), Madeira (4), Uatumã (6), Trombetas (8), and Tapajós (10). Gauging station locations are represented as *filled circles* and data was provided by Agência Nacional das Águas (ANA). *Stars* represent time of field data acquisition

have a neutral or basic pH, and are high in suspended sediments, and high in alkalinity (Konhauser et al., 1994). The Amazon River is 6,580 km long and, together with its approximately one thousand tributaries, drains a 6.5×10^6 km^2 area of South America. Seasonally, the Amazon discharge has a predictable monomodal fluctuation that results from the precipitation regimes in catchment areas of the large tributaries (Irion et al., 1997). The maximum and minimum discharge of the Amazon River, as measured at Óbidos (eastern-most gauging station), is reported as 203,000 m^3 s^{-1} at high water (June) and 91,700 m^3 s^{-1} at low water (December) (Richey et al., 1986). The Solimões River, as the Amazon River is called before its confluence with the Negro River, has several tributaries originating in the Andes and flowing through the lowlands. The Solimões drains an area of approximately 990,780 km^2 and the annual mean discharge is 103,000 m^2 s^{-1}. The Madeira River originates in the Bolivian Andes, and drains the Brazilian shield and the Central Amazon plain. It is the largest tributary of the Amazon River; and together with the Solimões River, represents the largest contributor of sediment to the Amazon River (Leite et al., 2011). The Madeira River drains an area of 1,420,000 km^2 with an annual discharge of 32,200 m^3 s^{-1} (Moreira-Turcq et al., 2003).

The Negro River has a drainage basin of 686,810 km^2 and is characterized by an annual mean discharge of 28,400 m^3 s^{-1} (Moreira-Turcq et al., 2003). The headwaters are in the Guyana Shield, and the drainage basin is associated with highly weathered lateritic and podsol soils. These hydromorphic soils are sandy, nutrient poor, and permeable. Rainfall interacts with forest litter and then percolates through these soils, transporting large quantities of dissolved organic matter into the rivers. The waters, therefore, tend to be acidic, rich in dissolved humic substances, and low in nutrients (Forsberg et al., 1988). The Uatumã River drains an area of approximately 70,600 km^2 and has a maximum discharge of approximately 1,370 m^3 s^{-1} in May/June. Uatumã's tributaries originate mostly in the Guiana Shield; as such, it has physical–chemical water characteristics similar to the Negro River.

The main tributaries of the Amazon lower course are the Trombetas (drainage area of 128,000 km^2 and mean discharge of 2,555 m^3 s^{-1}) and Tapajós (drainage area of 490,000 km^2 and mean discharge of 13,500 m^3 s^{-1}) rivers (Moreira-Turcq et al., 2003). Their headwaters are found in the highly weathered, low-gradient Guyana and Brazilian shields, respectively. These Precambrian shields are not undergoing strong physical erosion like that occurring in the Andes; and, therefore, have developed thick, clay-rich latosol soils. These soils retain water and organic matter for an amount of time sufficient to complete mineralization of dissolved organic matter. However, due to the intense chemical weathering that has produced these soils, dissolution of minerals is low, and waters draining from them remain low in dissolved solids. These rivers have low concentrations of suspended solids, are nutrient poor, and are characterized by high plankton production (Devol & Hedges, 2001).

Water samples

Sampling strategies for the field campaigns of 2005 (receding waters) and 2006 (rising waters) were as follows: in 2005, we collected subsurface (0.2 m depth) water samples at three different locations in each river, producing 27 discrete samples. In 2006, water samples were similarly collected at three different locations in each river, and additional samples were collected at the euphotic depth ($Z_{1\%}$), for a total of 66 discrete samples. For both sampling campaigns, we averaged data from the three different locations to represent a river. Immediately after sampling, water was vacuum-filtered onboard the boat, through pre-weighed and pre-ignited GF/F 0.7 µm glass-fiber membranes, for measuring the concentrations of TSS and photosynthetic pigments. Pigment samples were frozen at −80°C until HPLC analysis.

TSS was determined by weight difference following the method of APHA (1998). Pigments were determined by high-performance liquid chromatography (HPLC) using methods adapted from EPA (1997) and Mantoura & Repeta (1997). We quantified the following pigments using certified standards: chlorophyll *a* (Sigma-Aldrich Canada, Inc.) and *b*, zeaxanthin, alloxanthin, diadinoxanthin, peridinin, and fucoxanthin (DHI Water and Environment). The presence of these pigments was used as an indicator of assemblage of phytoplankton groups in the different rivers as per Wright & Jeffrey (2006), although the limitations are known due to the lack of reliable

published pigment ratios for defining fresh water phytoplankton assemblages (Descy et al., 2009). Just before HPLC analysis, the stored membranes were removed from the freezer, placed in centrifuge tubes with 90% acetone solution, ground, digested for 12 h while kept cold and dark, and then centrifuged. The extracts were filtered (0.45 µm membranes) into amber autosampler vials, and kept chilled and dark for imminent HPLC analysis. Analysis was done using a refrigerated autosampler, an injection volume of 200 µl, and a Summit P680A HPLC (Dionex, Oakville, ON, Canada) equipped with a programmable gradient pump, reverse-phase C_{18} analytical and guard columns (5 µm pore size, 120 Å, 4.6 × 250 mm), and a 1,000 channel photodiode array UV/VIS detector.

For determination of absorbance due to colored dissolved organic matter (CDOM), the filtrate that passed through 0.2 µm membrane was collected in pre-combusted amber glass bottles, and kept cold and dark in coolers. We subsequently analyzed the filtrate samples spectrophotometrically for absorbance at 440 nm using a 2000 USD spectrophotometer (Ocean Optics, Dunedin, FL, US) with a 100 mm cuvette, using Milli-Q water as a reference. The absorption coefficient of CDOM ($a_{\mathrm{CDOM}(440)}$ m^{-1}) was calculated from measured absorbance according to Kirk (1994):

$$a_{\mathrm{CDOM}(440)} = 2.303 A_{(440)}/L \quad (1)$$

where $A_{(440)}$ is the absorbance at 440 nm and L is the path-length of the cuvette in meters.

In situ optical data collection

At each of the 60 sampling locations (2005 and 2006 inclusive), we acquired vertical samples of planar irradiance with the HyperPRO radiometer (Satlantic, Halifax, NS, Canada) from subsurface to $Z_{1\%}$. The HyperPRO has an in-water hyperspectral radiometer (HyperOCR) to measure downwelling irradiance ($E_{\mathrm{d}(z,\lambda)}$), and sensors for temperature, depth, and tilt determinations. A second hyperspectral radiometer was installed on a pole on the top of the boat to measure the above-water downwelling irradiance ($E_{\mathrm{s}(\lambda)}$). Both radiometers operate in a calibrated spectral range from 350 to 800 nm at a 10 nm spectral resolution. All the measurements were simultaneously taken through a computer interface, and sensors were calibrated by the manufacturer just prior to data acquisition. The in-water $E_{\mathrm{d}(z,\lambda)}$ (180° field of view) was mounted on a horizontal plane (T frame). We mounted the profiling set on a downrigger on the side of the boat, which was always oriented to keep the sensors on the sunny side to avoid boat shading. The sensor was slowly lowered in a continuous manner to collect high rate vertical resolution (3 Hz sampling) data and to prevent significant tilt. Additionally, all the measurements were conducted at solar elevation between 45° and 65°, under relatively clear sky conditions, with wind speed lower than 2.0 m s^{-1} on average. The solar angle range allowed us to assume less than 10% difference in K_{d} values due to irradiance differences (Kauer et al., 2010).

Based on in situ measured $E_{\mathrm{s}(\lambda)}$ and $E_{\mathrm{d}(z,\lambda)}$, $Z_{1\%}$, the depth in which the downwelling irradiance at the PAR range falls to 1% of the surface irradiance at the PAR range, defined as the euphotic depth (Kirk, 1994), was measured in real time.

Processing of optical data

The raw data were filtered for tilt and synchronized with depth and time, and the normalized downwelling irradiance ($E'_{\mathrm{d}(z,\lambda)}$), the quantum irradiance over the PAR range ($q_{\mathrm{d}(\mathrm{PAR},z)}$), and the diffuse attenuation coefficient ($K_{\mathrm{d}(\lambda)}$) were calculated. $E'_{\mathrm{d}(z,\lambda)}$ was defined by normalizing $E_{\mathrm{d}(z,\lambda)}$ to the incident irradiance $E_{\mathrm{s}(\lambda)}$. We only considered data if the average coefficient of variance (CV) of $E_{\mathrm{s}(\lambda)}$ over the time of acquisition for the specific sample site was lower than 1%. High CVs were mostly due to broken cloudy conditions. The $E'_{\mathrm{d}(z,\lambda)}$ was then converted to percentage, thus representing light quality and avoiding possible interference of differences in light intensity. We further characterized the differences among the irradiance curves by defining the following indices: the wavelengths of maximum light at subsurface ($\lambda_{\mathrm{max\_surf}}$) and at $Z_{1\%}$ ($\lambda_{\mathrm{max\_Z1\%}}$), and the ratio in downwelling irradiance between 650 and 550 nm ($\lambda_{650/550}$) and 550 and 490 nm ($\lambda_{550/490}$). These ratios enabled us to capture the slope of the curves between the red-green and the green-blue parts of the spectra, respectively.

Quantum irradiance in the water column over the PAR range, $q_{\mathrm{d}(\mathrm{PAR},z)}$ in µmol m^{-2} s^{-1}, was defined as

$$q_{\mathrm{PAR}} = \int_{400}^{700} E_{\mathrm{d}}(\lambda)\frac{\lambda}{hc_0}\mathrm{d}\lambda \quad (2)$$

where λ is the wavelength of light, h is the Planck's constant 6.625×10^{-34} J s, and c_0 is the speed of light 3×10^8 m s^{-1} (Reinart & Arst, 1998).

$K_{d(\lambda)}$ was defined as the slope of the least-square regression of $\ln[E_{d(z,\lambda)}/E_{s(0-,\lambda)}]$ with respect to depth over the depth interval just below the water surface to $Z_{1\%}$, where most of the attenuation of solar energy takes place (Kirk, 2003). This is a commonly used method for a vertically homogenous water layer (Kirk, 2003; Paavel et al., 2006). The R^2 values of the linear regressions fit were consistently better than 0.98 for the 450–750 nm range. $K_{d(\lambda)}$ values were not calculated below 450 nm because $E_{d(z,\lambda)}$ decreased very quickly with depth, and the low irradiance levels were beyond the sensitivity of the instrument. This was particularly the case for rivers with high TSS concentrations, such as the Amazon, Solimões, and Madeira. Similar problems have been reported for high turbidity lakes in Estonia and Southern Finland (Reinart & Herlevi, 1996; Reinart et al., 2004; Paavel et al., 2006). We further removed the optical data acquired from the Madeira River in 2006 because of very low levels of measured $E_{d(z,\lambda)}$ and $E_{s(\lambda)}$ values. The $E_{s(\lambda)}$ values varied considerably and were much lower than expected for equatorial regions. We can only speculate that there were technical issues at the time in which measurements were taken. Field notes in regard to maneuvering of the boat attest to that.

In order to analyze the influence of the water optical constituents on spectral K_{ds} variability, we defined the statistical relationships (1) among the spectral $K_{ds,}$ and (2) among spectral K_{ds} and optical water constituents. All analyses were conducted at a 99% significance level.

Results

Hydrological setting and water temperature

Figure 1 shows time series of monthly water level and precipitation at the sampled rivers (data from Agência Nacional das Águas-ANA), between January 2005 and December 2006. The water level for the Amazon River is represented by data from Óbidos station, which is the most downstream gauging station in this river. The rivers show a monomodal variation in the water level, with generally higher waters occurring in April–May and lower in October–November. The variations in water level are regulated by the seasonal distribution of rainfall in the catchment area of the rivers, with a general delay of about 2 to 3 months between the start of the rainy season and the river beginning to rise—generally in November–December (Irion et al., 1997). Our sampling campaigns happened after the 2005 maximum (onset of the receding waters and the dry season) and the 2006 minimum (onset of the rising waters and after the onset of the wet season) (Fig. 1). Of special note is the below average rainfall in the beginning of 2005, which caused rivers to drop to recorded low water levels. This was the second most severe drought to occur in the century, exceeded only by the drought of 2010 (Marengo et al., 2011).

During both sampling periods, the temperature profiles (measured $\pm$ 3 h of the solar noon) from the surface to $Z_{1\%}$ showed a 30°C average, and mostly within 0.3°C of the surface temperature (Table 1).

Optically active constituents

While the concentrations of water optical constituents, TSS, Chla, and $a_{CDOM(440)}$, at surface and at $Z_{1\%}$ were similar due to the well-mixed euphotic layer, the variation in concentrations among rivers and between the two seasons were noteworthy (Table 1). These variations are in the same range reported by other researchers (see Table 2 for comparisons). The reduced number of comparisons with other studies is related to differences in sampling procedures and periods of the hydrological cycle. For instance, several authors report concentrations derived from integrated depth sampling (Meade, 1994; Dunne et al., 1998; Leite et al., 2011). This can result in large variability in published concentrations. For example, in the case of TSS, the Amazonian rivers show concentrations that are many times higher closer to the river bed than at the surface (Meade, 1994).

The overall range of measured TSS was 1.6–66.9 and 3.2–217.2 mg l^{-1} for 2005 and 2006, respectively. The seasonal increase in TSS mostly happened in the Amazon, Solimões, and Madeira Rivers (an average 46 and 150.0 mg l^{-1}, respectively, for 2005 receding and 2006 rising). TSS also increased in the Tapajós River in 2006 (4.1 mg l^{-1}) compared with 2005 (1.6 mg l^{-1}). Concentrations in the Negro and Trombetas Rivers remained similar, whereas they decreased considerably in the Uatumã River in 2006 compared with 2005. The highest TSS waters were

Table 1 Optically active constituents and downwelling diffuse attenuation coefficients data

Rivers	Negro	Solimões	Amazon 1	Madeira	Amazon 2	Uatumã	Amazon 3	Trombetas	Tapajós	Amazon 4
2005 receding										
Chla (μg/l)	1.8 (0.6)	0.3 (0.1)	0.3 (0.0)	0.5 (0.0)	0.3 (0.0)	1.2 (0.1)	–	2.7 (0.1)	2.1 (0.1)	0.5 (0.0)
TSS (mg/l)	3.2 (0.4)	66.9 (37.2)	17.9 (4.6)	52.5 (2.2)	41.1 (18.3)	12.1 (2.5)	–	3.3 (1.2)	1.6 (0.3)	57.4 (5.6)
a_{CDOM} (m^{-1})	10.7 (0.2)	5.1 (0.4)	10.6 (2.6)	4.0 (0.0)	7.0 (0.3)	6.4 (0.3)	–	4.7 (0.5)	1.6 (0.1)	5.9 (0.4)
T (°C)	29.5 (0.2)	29.7 (0.0)	29.5 (0.0)	30.6 (0.0)	30.1 (0.1)	29.9 (0.0)	–	29.6 (0.3)	30.6 (0.0)	30.4 (0.0)
Z_{eu} (m)	1.9 (0.1)	1.1 (0.1)	1.2 (0.0)	0.9 (0.1)	1.1 (0.1)	1.9 (0.1)	–	2.9 (0.2)	5.6 (0.5)	1.0 (0.0)
K_{d_B} (m^{-1})	5.4 (0.0)	6.6 (0.5)	8.6	8.1 (0.7)	6.4 (0.2)	5.2 (0.3)	–	3.0 (0.4)	1.3 (0.0)	5.7 (0.2)
K_{d_G} (m^{-1})	4.4 (0.2)	4.6 (0.4)	5.1	5.9 (0.5)	4.8 (0.7)	3.3 (0.1)	–	2.0 (0.2)	0.8 (0.0)	4.2 (0.8)
K_{d_R} (m^{-1})	2.1 (0.0)	3.1 (0.3)	3.0	4.1 (0.3)	3.2 (0.5)	2.0 (0.1)	–	1.3 (0.2)	0.7 (0.0)	3.0 (0.7)
$\lambda_{max\_Z1\%}$(nm)	690	685	690	680	685	690	–	690	575/640	685
2006 rising										
Chla (μg/l)	0.6 (0.2)	0.3 (0.0)	0.3 (0.0)	0.6 (0.0)	0.4 (0.0)	4.2 (0.6)	0.3 (0.0)	1.5 (0.1)	16.3 (7.2)	0.5 (0.1)
TSS (mg/l)	3.6 (0.6)	173.0 (8.4)	139.1 (20.4)	217.2 (5.6)	120.5 (16.6)	4.5 (0.9)	134.1 (5.9)	3.2 (0.2)	4.1 (0.6)	138.8 (5.4)
a_{CDOM} (m^{-1})	10.3 (0.5)	1.9 (0.1)	3.6 (0.3)	1.6 (0.7)	3.0 (0.2)	1.5 (0.2)	2.6 (0.2)	1.5 (0.1)	2.1 (0.1)	2.6 (0.2)
T (°C)	–	30.6 (0.0)	30.9 (0.0)	31.4 (0.0)	31.0 (0.0)	31.5 (0.4)	30.9 (0.0)	31.9 (0.1)	30.8 (0.0)	30.9 (0.0)
Z_{eu} (m)	5.4 (1.2)	0.5 (0.0)	0.5 (0.1)	0.5 (0.1)	0.5 (0.0)	3.8 (0.6)	0.5(0.0)	4.1 (0.2)	2.6 (0.4)	0.5
K_{d_B} (m^{-1})	–	14.5 (2.7)	12.2 (3.9)	–	11.8 (2.0)	2.4 (0.4)	10.3 (3.0)	2.0 (0.2)	3.0 (0.5)	15.1 (2.6)
K_{d_G} (m^{-1})	–	11.2 (2.0)	10.1 (2.0)	–	10.0 (1.4)	1.4 (0.3)	9.2 (4.1)	1.2 (0.1)	1.9 (0.3)	13.5 (1.6)
K_{d_R} (m^{-1})	–	9.4 (1.5)	8.4 (1.4)	–	7.3 (0.9)	1.0 (0.2)	9.5 (2.8)	1.0 (0.1)	1.7 (0.3)	9.7 (1.6)
$\lambda_{max\_Z1\%}$(nm)	–	695	695	–	695	585/650/690	690	585/640/690	580/650/695	690

Values represent mean of triplicates and values between brackets represent one standard deviation of the mean. Note that some rivers showed more than one $\lambda_{max\_Z1\%}$

Table 2 Comparison of concentration of optical water constituents in Amazonian rivers according to different studies

Source	Water stage	Negro	Solimões	Amazon	Madeira	Uatumã	Trombetas	Tapajós
This study	Receding	1.8/3.2	0.3/66.9	0.3/40.0	0.5/52.5	1.2/2.1	2.7/3.3	2.1/1.6
	Rising	0.6/3.6	0.3/173.0	0.3/133.0	0.6/217.2	4.2/4.5	1.5/3.2	18.3/4.1
Moreira-Turcq et al. (2003)	Receding	–/8.8	–/17.6	–	–/51.1	–	–/15.8	–/2.0
	Rising	–/4.0	–/127.1	–	–	–	–/14.8	–/3.5
Putz & Junk (1997)	Receding	4.0/–	–	–	–	–	–	–
	Low	2.0/–	–	–	–	–	–	–
Dustan (2009)	High-receding	–	–	0.5/–	–	–	–	–
Fisher (1979)	Low	2.0/–	–	0.5/–	–	–	–	–
Rudorff et al. (2009)	Receding	–	–	2.0/40.0	–	–	–	3.4/1.0

Concentrations are expressed as Chla (μg l^{-1})/TSM (mg l^{-1}). Note that for the same reference, data is not available for all rivers. Also, all concentrations represent surface samples

found in the rivers with headwaters in the Andean Cordillera: Solimões, Madeira, and Amazon Rivers. Maximum concentrations (>170.0 mg l^{-1}) in the Solimões and Madeira Rivers happened at rising waters (2006), with minimum concentrations (~50.0 mg l^{-1}) at receding waters (2005). The low TSS waters (approximately 3.0 mg l^{-1}) were found in rivers with headwaters in the Brazilian and Guyana shields: the Negro, Uatumã, Trombetas, and Tapajós Rivers. One exception was the Uatumã waters in 2005, in which TSS reached 12.1 mg l^{-1}. This high concentration was likely a result of mixing with Amazon River waters through myriad water pathways of the wide floodplain.

Measured $a_{CDOM(440)}$ values varied markedly among the different rivers and seasonally. Observed ranges were from 1.6 to 10.7 and 1.5 to 10.3 m^{-1} for 2005 and 2006 waters, respectively (Table 1). Among the sampled rivers, the highest $a_{CDOM(440)}$ values were measured in the Negro (10.7 and 10.3 m^{-1} for 2005 receding and 2006 rising waters, respectively) and at the Amazon after the confluence of the Negro and Solimões (10.6 m^{-1} for 2005 receding). Intermediate values were measured in the Solimões, Amazon, Uatumã, and Madeira (~4.5 m^{-1}), and the lowest values were measured in the Trombetas and Tapajós (3.2 and 1.8 m^{-1} for 2005 receding and 2006 rising waters, respectively). The lower dissolved organic matter in the waters of the Solimões, Madeira, and Amazon Rivers compared with, for instance, the Negro River, is a result of the high adsorption and decomposition rates in the soil, groundwater inputs, seepage from fringing wetlands, and in-channel processes in these rivers (McClain et al., 1997). The high dissolved organic matter of the Negro River is typical of Amazonian rivers draining highly weathered lateritic and podsol soils (Forsberg et al., 1988). The Tapajós River showed one of the lowest $a_{CDOM(440)}$ values (1.6 m^{-1}) at receding waters, typical of Amazonian rivers that drain highly weathered, low-gradient shield regions (Devol & Hedges, 2001; Moreira-Turcq et al., 2003).

Contrary to the TSS and $a_{CDOM(440)}$ trends, the Tapajós River exhibited the highest Chla concentrations, especially at the rising water stage. Generally, at receding water stage, Chla values were higher in the Tapajós and Trombetas rivers (2.1 and 2.7 μg l^{-1}, respectively), and in the Negro and Uatumã rivers (1.8 and 1.2 μg l^{-1}). The concentrations increased considerably at rising waters in the Tapajós (~18.3 μg l^{-1}) and Uatumã (4.2 μg l^{-1}), while they remained approximately the same in the Trombetas River (1.5 μg l^{-1}) and decreased in the Negro River (0.6 μg l^{-1}). The waters of the Amazon, Solimões, and Madeira exhibited the lowest Chla values (~0.4 μg l^{-1}) during both sampling periods (Table 1).

Figure 2 and Table 3 show the distribution patterns of the following biomarker pigments: fucoxanthin, diadinoxanthin, peridinin, Chlb, alloxanthin, and zeaxanthin. Overall, the pigment concentrations and diversity were higher in the waters of the Tapajós (highest concentrations), Trombetas, Negro, and Uatumã rivers. These waters exhibited higher concentrations of zeoxanthin (indicating the presence of Cyanophyceae), fucoxanthin, and diadinoxanthin pigments (diatoms), as well as alloxanthin pigment (Cryptophytceae), Chlb (Chlorophyceae), and peridinin (Dinophyceae) (Wright & Jeffrey, 2006), compared with waters from the

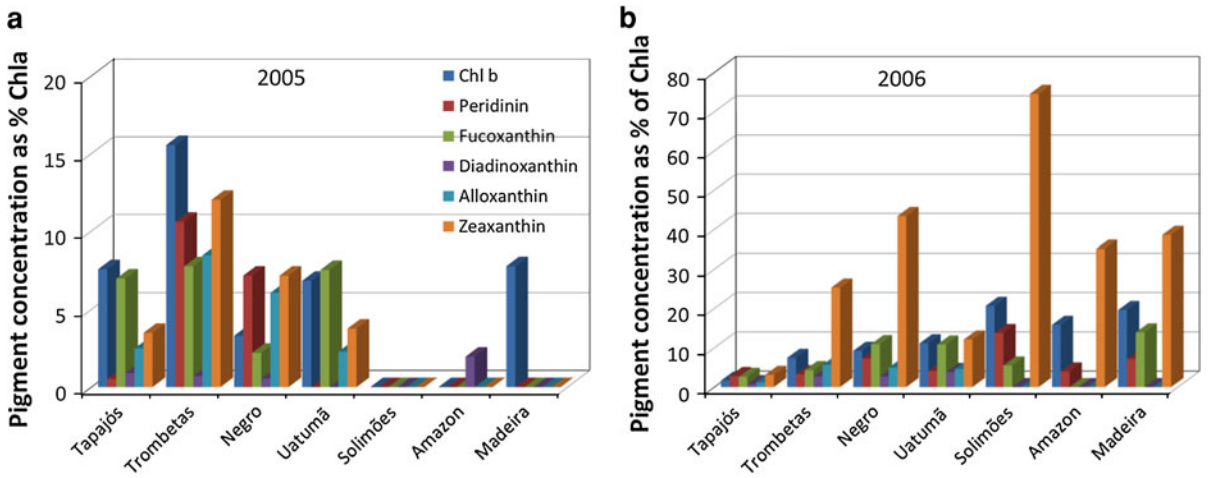

Fig. 2 Pigment distribution expressed in relative abundance in relation to Chla for the different Amazonian rivers. **a** 2005 data—receding waters and **b** 2006 data–rising waters. Note the different magnitude of the *y* axis

Table 3 Pigment concentrations (μg l^{-1}) for the different Amazonian rivers collected in 2005 (receding) and 2006 (rising waters)

Rivers	Tapajós	Trombetas	Negro	Uatumã	Solimões	Amazon	Madeira
2005 receding							
Chla	2.1	2.7	1.8	1.2	0.3	0.3	0.5
Chlb	0.2	0.2	0.06	0.08	n.d.	n.d.	0.04
Peridinin	0.01	0.01	0.01	n.d.	n.d.	n.d.	n.d.
Fucoxanthin	0.1	0.1	0.1	n.d.	n.d.	n.d.	n.d.
Alloxanthin	0.07	0.2	0.1	0.04	n.d.	n.d.	n.d.
Zeaxanthin	0.3	0.1	n.d.	0.05	n.d.	n.d.	n.d.
2006 rising							
Chla	16.3	1.5	0.6	4.2	0.3	0.4	0.6
Chlb	0.3	0.1	0.05	0.5	0.06	0.07	0.1
Peridinin	0.5	0.05	0.04	0.2	0.04	0.02	0.04
Fucoxanthin	0.4	0.06	0.06	0.5	0.02	n.d.	0.09
Diadinoxanthin	0.1	0.04	0.01	0.2	n.d.	n.d.	n.d.
Alloxanthin	0.2	0.1	0.03	0.2	n.d.	n.d.	n.d.
Zeaxanthin	0.5	0.4	0.3	0.5	0.2	0.2	0.2

n.d. stands for not detected

Amazon, Madeira, and Solimões. For these rivers, biomarker pigment concentrations were very low or generally below the detection limit, except for zeaxanthin (dominant), Chlb, peridinin, and fucoxanthin in some stations, and only at rising water stage, thus indicating the presence of Cyanophyceae, Chlorophyceae, Dinophyceae, and Bacillariophyceae, respectively (Wright & Jeffrey, 2006). Our results on pigment diversity are consistent with data reported in Saliot et al. (2001) for similar rivers, thus confirming lower diversity and concentrations of pigments in the Amazon, Madeira, and Solimões, and higher diversity and pigment concentrations in the Trombetas, Uatumã, and Negro, with the highest in the Tapajós River.

Light climate

The light climate of the different water types was analyzed according to the depth at which the downwelling irradiance at the PAR range falls to 1% of the

surface irradiance, the normalized in-water irradiance, the quantum irradiance over the PAR range, and the diffused attenuation coefficient (Table 1; Figs. 3, 4, 5, respectively).

$Z_{1\%}$ varied at two different times of the year and for the different rivers (Table 1). At the receding waters of 2005, $Z_{1\%}$ ranged between 0.9 and 1.9 m in the waters of the Amazon, Madeira, and Solimões, and the waters of the Negro and Uatumã rivers, respectively, compared with 2.9–5.6 m in Trombetas and Tapajós. At the rising waters of 2006, $Z_{1\%}$ generally decreased to about half of the depth measured in the receding waters of 2005, except for the Negro, Uatumã, and Trombeta rivers, where $Z_{1\%}$ was higher.

Variations in the normalized downwelling irradiance ($E'_{d(z,\lambda)}$) at subsurface (0.2 m) and reaching $Z_{1\%}$ for the different rivers and seasons are shown in Fig. 3. The shape and magnitude of the irradiance curves differed for the various rivers and the two different sampling periods. At receding waters, the Uatumã, Negro, Amazon, Solimões, Madeira, and Trombeta rivers were characterized by a λ_{max} at approximately 680–690 nm for both depths, subsurface (Fig. 3a) and $Z_{1\%}$ (Fig. 3b); while for the Tapajós River, it was around 575 nm with secondary peaks at 640 and 690 nm at $Z_{1\%}$. At subsurface, the $\lambda_{650/550}$ and $\lambda_{550/490}$ of the sampled rivers indicated that generally red irradiance was about 50% higher than green irradiance, and green irradiance was about two times higher than blue irradiance, respectively. Contrastingly, for the Tapajós River, irradiance values at 490, 550, and 650 nm were similar, thus producing a flatter curve (Fig. 3a).

At $Z_{1\%}$, the irradiance curves (Fig. 3b) showed different steepnesses when compared with the subsurface curves (Fig. 3a). The $\lambda_{550/490}$ indicated blue irradiance generally much lower than green, often more than ten times lower. The $\lambda_{650/550}$ showed strong depletion of green light, about five times less green light compared with red light. Again, the exception was the Tapajós River, where values of E'_d at 650 and 550 nm were similar, and noticeable minimums were defined at 620 and 670 nm (Fig. 3b).

At rising waters, the irradiance curves showed differences in the quality of spectral light in the Uatumã, Trombetas, and Tapajós Rivers when compared with receding waters. In these rivers, $E'_{d(\lambda)}$ exhibited three maximum wavelengths at approximately 585, 645, and 690 nm, while high TSS rivers remained with one maximum, both at subsurface (Fig. 3c) and $Z_{1\%}$ (Fig. 3d). In these waters, $\lambda_{650/550}$ revealed that red and green light had almost similar magnitude at subsurface, while red irradiance was about five times higher than green at $Z_{1\%}$. The largest irradiance differences between the sampling periods occurred for the Uatumã and Trombetas Rivers, where the profile of the subsurface $E'_{d(\lambda)}$ at rising waters resembled the Tapajós River—similar λ_{max}, $\lambda_{650/550}$, and $\lambda_{550/490}$. At $Z_{1\%}$, $E'_{d(\lambda)}$ curves showed more pronounced differences, with dominant green light availability in the waters of the Uatumã, Tapajós, and Trombetas Rivers (Fig. 3d).

The next set of data corresponds to the quantum irradiance over the PAR range ($q_{d(PAR,z)}$) for the different rivers at the two sampling periods. In order to allow for adequate comparative analysis of $q_{d(PAR,z)}$, we first evaluated all the measured above-water quantum irradiance over the PAR range $q_{s(PAR)}$. On average, $q_{s(PAR)}$ values were 1,800 μmol m^{-2} s^{-1} (average difference among sites was 11%) and 1,686 μmol m^{-2} s^{-1} (difference among sites was 15%) for 2005 and 2006, respectively. The high and similar $q_{s(PAR)}$ values for both sampling periods were expected because light intensity near the equator is mostly constant year around (Junk & Krambeck, 2000), and the optical measurements were conducted with a narrow solar angular range around noon. The similarity between measured $q_{s(PAR)}$ values for 2005 and 2006 allowed us to assume that the changes in $q_{d(PAR,z)}$ were related to the optical water constituents and not changes in illumination conditions. High TSS waters exhibited the lowest $q_{d(PAR,z)}$ (Fig. 4a, b), especially in 2006 (<41.1 μmol m^{-2} s^{-1} at the depth of half $Z_{1\%}$) when the TSS concentrations were the highest. In 2005, quantum irradiance was approximately 180.0 μmol m^{-2} s^{-1} for the Uatumã and Negro, and 220.0 μmol m^{-2} s^{-1} for the Tapajós and Trombetas (Fig. 4a). In 2006, the quantum irradiance values in the Tapajós decreased to approximately 80.5 μmol m^{-2} s^{-1}, while the Trombetas and Uatumã remained similar (Fig. 4b).

The last set of data corresponds to the spectral diffuse attenuation coefficients for downward irradiance ($K_{d(\lambda)}$) for 2005 (Fig. 5a) and 2006 (Fig. 5b). Overall, attenuation was higher in the blue part of the spectra, decreasing toward the green, and increasing slightly into the near infrared spectra (>700 nm). For

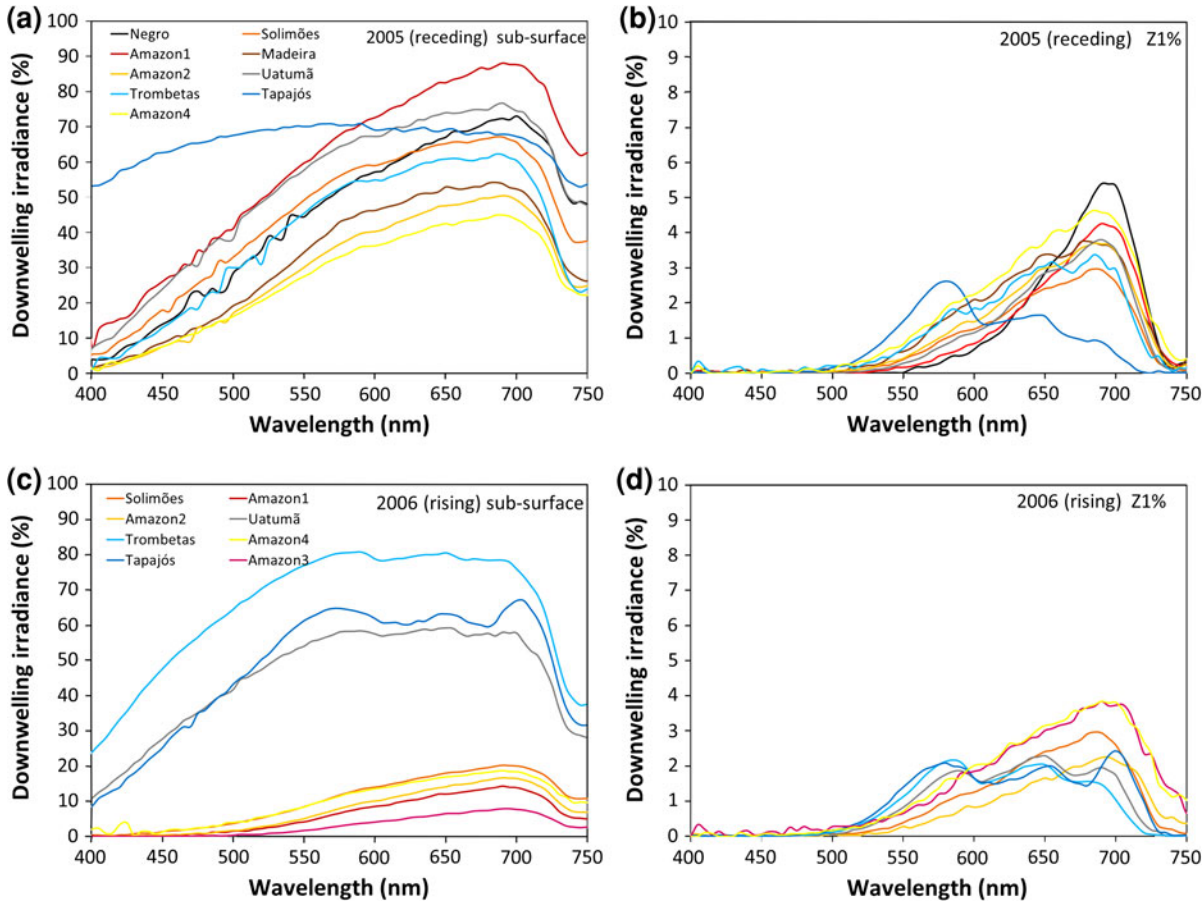

Fig. 3 Downwelling irradiance relative to incoming light representative for the sampled Amazonian rivers. **a** 2005—receding waters at sub-surface, **b** 2005—receding waters at $Z_{1\%}$, **c** 2006—rising waters at sub-surface, and **d** 2006—rising waters at $Z_{1\%}$. Note the magnitude difference between irradiance at sub-surface and $Z_{1\%}$

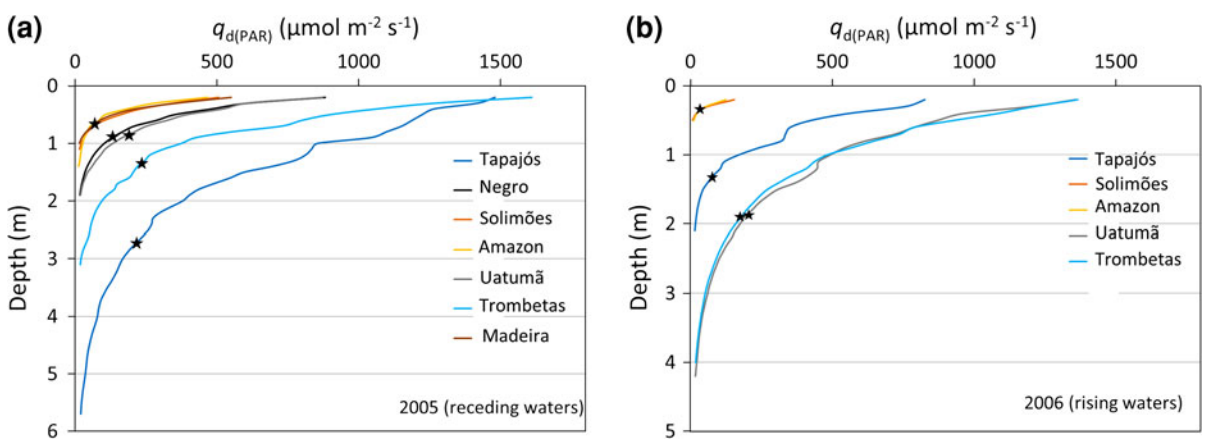

Fig. 4 Quantum irradiance over the PAR range, $q_{d(PAR,z)}$, in µmol m^{-2} s^{-1} for sampled Amazonian rivers. **a** Receding waters—2005 and **b** rising waters—2006. *Stars* represent the depth of half $Z_{1\%}$

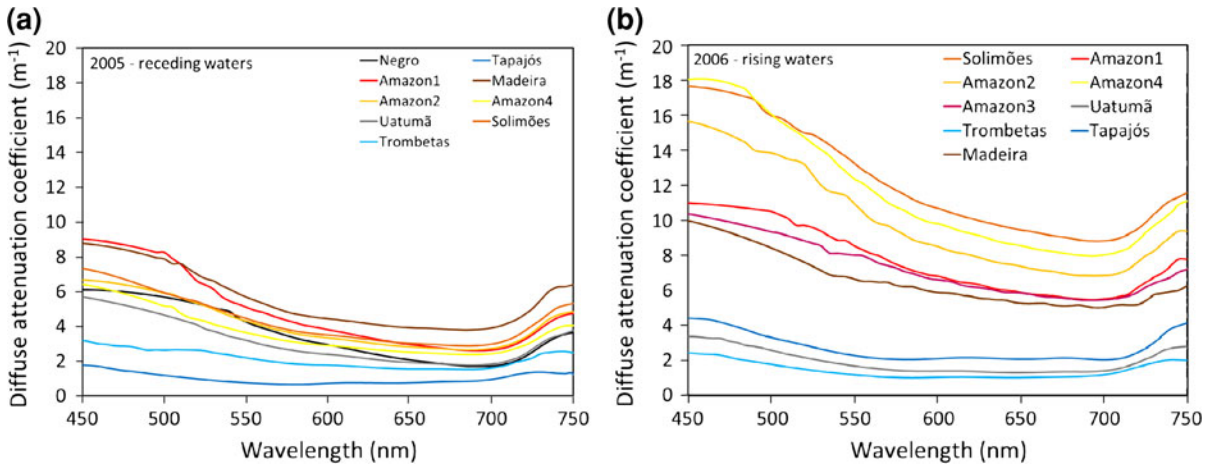

Fig. 5 Diffuse attenuation coefficient ($K_{d(\lambda)}$). **a** Receding waters—2005 and **b** rising waters—2006

ease of presenting the K_d behavior, we show three representative wavelengths, 490 (K_{d_B}), 550 (K_{d_G}), and 650 nm (K_{d_R}) (Table 1). For both sampling periods, spectral K_d values were higher for the Amazon, Madeira, and Solimões compared with the waters of the Tapajós, Trombetas, Uatumã, and Negro. At the receding waters of 2005, K_{d_B} exhibited the highest values, decreasing in about the same magnitude toward the green and red wavelengths, except in the Tapajós River, where K_{d_G} and K_{d_R} were similar. At the rising waters of 2006, K_d values were generally higher in any part of the spectra and the differences between spectral K_{ds} were lower compared with the 2005 coefficients.

We statistically correlated K_{d_B}, K_{d_G}, and K_{d_R} with the predictor variables, $a_{CDOM(440)}$, TSS, and Chla, to define the influence of the optical water constituents on K_d variability. Predictor variables were only accepted in the regression models at $P < 0.01$. The models were developed for the following group of data: (i) all data combined (high and low TSS waters); (ii) only low TSS waters (Negro, Uatumã, Tapajós, and Trombetas); and (iii) only high TSS waters (Amazon, Madeira, and Solimões). The division of high and low TSS waters was done due to the K_d differences between these waters, especially in the red wavelengths (Fig. 5). K_d values at the red wavelengths for the high TSS waters are systematically higher than 2.0 m^{-1} compared with low TSS waters (Fig. 6c). This threshold is not well defined in the blue and green part of the spectra because of the effects of high CDOM absorption and inorganic particulate scattering on the attenuation coefficients at these wavelengths. For instance, the high CDOM waters of the Negro River show K_d values similar to the Amazon River at the blue and green wavelengths, but lower K_d at red wavelengths where CDOM does not absorb light efficiently (Fig. 5a). Table 4 shows the coefficient of determination of linear regressions between spectral K_{ds} and water optical constituents.

The statistical analysis indicated that when all the data were included (all rivers, both seasons), the fit of the K_d models was the highest ($r = 0.92$–0.93) and TSS was the significant predictor variable. However, a closer analysis of the K_d variability of the Negro, Uatumã, Tapajós, and Trombetas suggests that the statistical models are not good predictors of the K_d for these waters, in turn suggesting that some optical constituent other than TSS alone defined light attenuation at these waters. Accordingly, the K_d models generated with only low TSS waters defined $a_{CDOM(440)}$ as the significant predictor variable (Table 4), in particular, as expected, for light attenuation in the green ($r = 0.94$) and blue ($r = 0.89$) wavelengths. The statistical relationship between K_{d_R} and $a_{CDOM(440)}$ decreased ($r = 0.74$), likely due to the diminished influence of absorption by CDOM at red wavelengths. The K_d models generated for high TSS waters were mainly described by TSS ($r = 0.84$ for all models), but $a_{CDOM(440)}$ had a significant secondary negative correlation ($r = -0.62$ and -0.68) (Table 4). This negative correlation is a result of the dominant influence of TSS scattering on the K_d values of these waters. The highest TSS waters (highest K_{ds}), such as at the Amazon River at rising waters, are

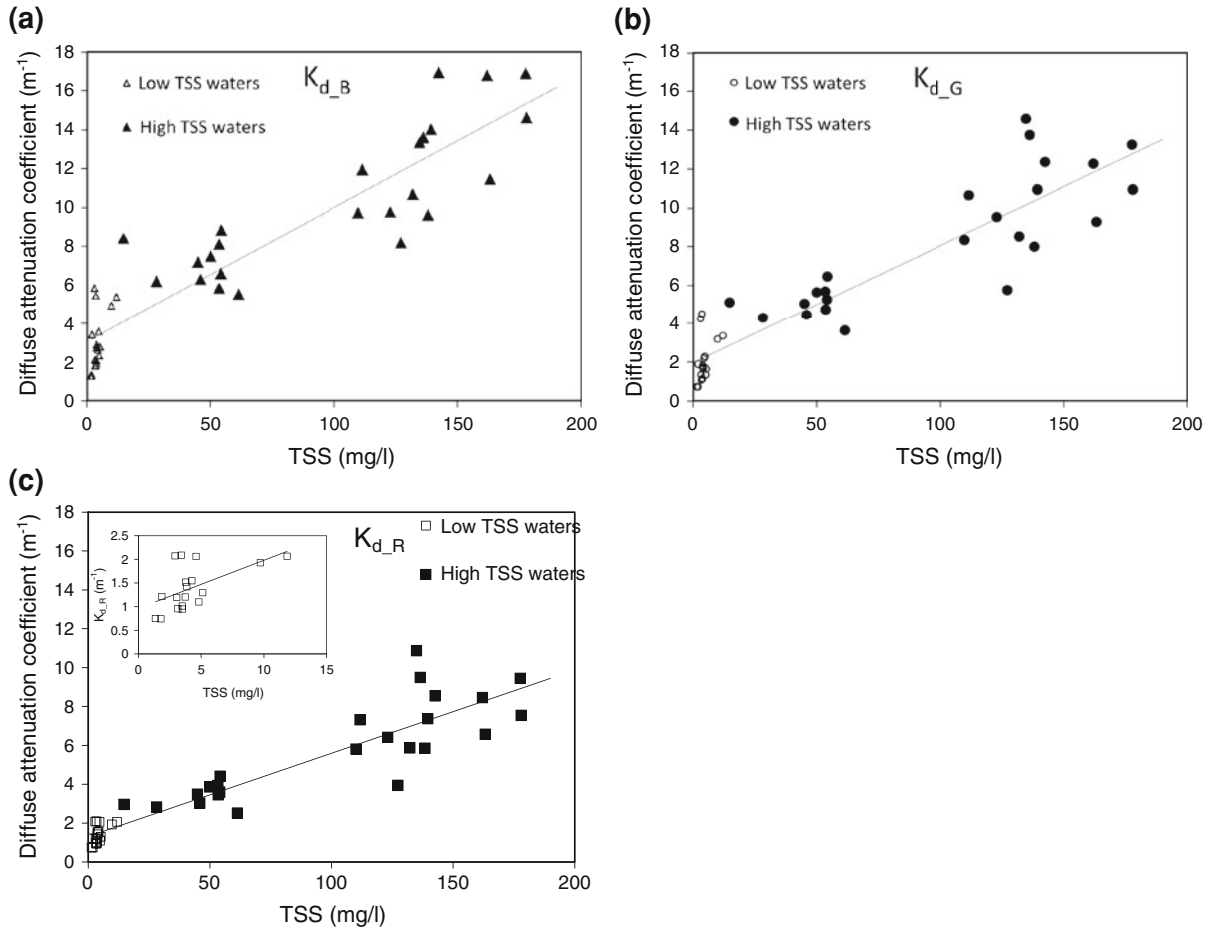

Fig. 6 Relationship between diffuse attenuation coefficient (m^{-1}) and total suspended matter (mg l^{-1}) for all sampled rivers (2005 and 2006). **a** K_{d_B} (490 nm), **b** K_{d_G} (550 nm), and **c** K_{d_R} (650 nm). Regression line was defined considering data from all the rivers. *Dark filled symbols* represent only high TSS waters and *open symbols* represent low TSS waters. Note the lower variability of K_{ds} in low TSS waters compared with high TSS waters, especially at 650 nm (*inset* graphic in **c**)

associated with lower $a_{CDOM(440)}$ values compared with lower TSS waters such as at Amazon River at receding waters (lowest K_{ds}), which have higher $a_{CDOM(440)}$. The relationship between TSS and K_d does not reveal a saturation point for the measured TSS range ($\sim$20.0–173.0 mg l^{-1}, both sampling periods) (Fig. 6). This is in agreement with current knowledge of K_d (and scattering) variability with TSS for the similar TSS range reported here (Squires & Lesack, 2003; Loisel et al., 2007; Boss et al., 2009; Sun et al., 2009).

Discussion

Based on temporal (receding and rising sampling periods) and spatial (eight large rivers) in situ data, we analyzed optical variables that describe the underwater light field and their relationship with water constituents of Amazonian fluvial environments. We found that the spectral light attenuation; and, therefore, the quality and quantity of spectral light, differ among sampled rivers and between seasons as a result of the optical constituents in the water, which in turn are a result of the source, physical processes, and biogeochemical reactions in the rivers' sub-basin, and water mixing between rivers (Devol & Hedges, 2001).

In the sampled Amazonian rivers with headwaters in the Andean Cordillera (Solimões, Madeira, and Amazon Rivers), light attenuation limits the 1% level of PAR to depths shallower than 1.0 m, especially at the rising water stage. At the depth of half of $Z_{1\%}$, quantum irradiance over the PAR spectra was the

Table 4 Correlation results for the K_{ds} and optical water constituents

	K_{d_B}	K_{d_G}	K_{d_R}
All data ($N = 42$)			
K_{d_B}	1.0		
K_{d_G}	0.97*	1.0	
K_{d_R}	0.96*	0.99*	1.0
Chla	−0.38	−0.37	−0.33
$a_{CDOM(440)}$	−0.04	−0.07	−0.16
TSS	0.92*	0.92*	0.93*
Low TSS ($N = 18$)			
K_{d_B}	1.0		
K_{d_G}	0.97*	1.0	
K_{d_R}	0.92*	0.91*	1.0
Chla	−0.02	−0.1	0.3
$a_{CDOM(440)}$	0.89*	0.94*	0.74*
TSS	0.55	0.43	0.56
High TSS ($N = 24$)			
K_{d_B}	1.0		
K_{d_G}	0.93*	1.0	
K_{d_R}	0.91*	0.99*	1.0
Chla	−0.08	0.01	0.05
$a_{CDOM(440)}$	−0.62*	−0.65*	−0.68*
TSS	0.84*	0.84*	0.84*

* Correlation is significant at the 0.01 level

lowest among all the sampled rivers: 106.2 and 41.1 μmol m^{-2} s^{-1} for receding and rising waters, respectively (Fig. 4). Since quantum irradiance is attenuated differently in different parts of the spectrum, the wavelength composition of the irradiance changes with depth. Vertically, in these waters, the $Z_{1\%}$ depth for blue light was approximately at 0.5 m or shallower, green light was present in very low intensities, and red light was the least absorbed and, therefore, defined the available quantum irradiance at $Z_{1\%}$ (Fig. 3b). The spectral dependence of light intensity with depth is dominantly due to light attenuation by both TSS scattering and CDOM absorption processes, with the latter generally more wavelength dependent. Together, these processes defined the highest K_d values among all the sampled rivers. Specifically, the scattering magnitude is a function of the high concentrations and the dominant inorganic nature of the suspended particulates (Moreira-Turcq et al., 2003), and therefore characterized by a high index of refraction. The mean K_d values were maximal at rising waters, 12.7, 10.1, and 9.1 m^{-1} for blue, green, and red light, respectively, when TSS was the highest (Table 1). These values are among the highest reported for turbid waters (Table 5). As TSS concentrations decreased at receding waters, so did the spectral K_{ds} (7.0, 4.9, and 3.3 m^{-1} for blue, green, and red spectra, respectively). Slightly lower measured K_d values of sediment-laden waters only happened when low TSS tributaries, such as the Tapajós River, mixed with the waters of the Amazon River. For instance, for the Amazon 4 station at receding water stage, K_d values were $K_{d\_B} \sim 5.7$ m^{-1}, $K_{d\_G} \sim 4.2$ m^{-1}, and $K_{d\_R} \sim 3.0$ m^{-1} as a result of mixing with the low TSS waters of the Tapajós River.

Seasonal and inter-annual variability of light attenuation is expected for these waters due to variability in TSS and DOM concentrations. The seasonality in TSS concentrations is related to the rivers' discharge and described by the clockwise loop pattern (Meade, 1994; Leite et al., 2011). For instance, as the waters of the Madeira and Amazon rivers begin to rise, high TSS concentrations (>100.0 mg l^{-1}) are observed as a result of resuspension of fine-grained sediment from the river banks, channel, and floodplain (Meade, 1994). According to the clockwise loop pattern, at receding waters, TSS concentrations ($\sim$50.0 mg l^{-1}) are close to the yearly lowest, which are observed at the lowest water stages (Leite et al., 2011). Additionally, at receding waters, an increased TSS downstream trend was also observed, likely associated with the resuspension of sediment due to changes in the surface slope of the main stem of the Amazon, which is a result of slightly different timing of peak water stages of the Amazon River and some of its tributaries (Dunne et al., 1998; Meade, 2007) and the exchange of sediments between the channel and floodplain (Dunne et al., 1998).

Dissolved organic matter also varies seasonally in these sediment-laden rivers. At the receding water stage, in the Amazon mainstem channel, starting at the sampling station downstream from the confluence of the Solimões and Negro Rivers (Amazon 1 station—Fig. 1), high inputs of CDOM from the high discharge waters of the Negro River resulted in high $a_{CDOM(440)}$ measurements (Amazon 1 $a_{CDOM(440)} = 10.6$ m^{-1}). Further downriver, mixing processes and loss of humic and fulvic acids due to sorption onto fine suspended particles of sediment-laden rivers (Ertel et al., 1986) resulted in a downstream decrease of

Table 5 Comparison of diffuse attenuation coefficient in aquatic systems according to different studies

Source	$K_{d\_490}/K_{d\_550}/K_{d\_650nm}$ (m^{-1})	$K_{d(PAR)}$ (m^{-1})	Location	Water conditions	Classification
This study	7.0/4.9/3.3	–	Amazonian rivers	49.2/6.5/0.4	High TSS
	12.7/10.1/9.1			154.6/2.6/0.4	
This study	5.4/4.4/2.1	–	Negro River	3.2/10.7/1.8	High CDOM
This study	1.3/0.8/0.7	–	Tapajós River	1.6/1.6/2.1	High Chla
	3.0/1.9/1.7			4.1/2.1/18.3	
Kauer et al. (2010)	0.7/0.5/0.7	–	Estonia lakes	–	Low Chla
	6.0/3.0/3.0	–	Estonia lakes	–	High Chla
	8.0/5.0/2.0	–	Estonia river		High DOM
Arst et al. (2008)	–	~3.0	Estonia lakes	–	High Chla
Reinart et al. (2004)	5.5/3.5/2.5	–	Estonia lakes	–/–/~50.0	Turbid
	2.0/1.0/1.0	–	Estonia lakes	1.7/4.9[a]/6.9	Mesotrophic
Squires & Lesack (2003)	–	~7.0	Mackenzie Delta lakes	~125.0/–/–	High TSS
	–	~4.0		~50.0/–/–	High TSS
Furch et al. (1985)	–	~1.0	Amazonian lake	~3.0/–/–	High CDOM
	–	~7.0	Amazonian lake	~100.0/–/–	High TSS

Note that some data are shown as $K_{d(PAR)}$, others as spectral K_{ds}. Spectral K_{ds} are presented as $K_{d\_490}/K_{d\_550}/K_{d\_650nm}$. Water condition are represented as TSS (mg l^{-1})/$a_{CDOM(440)}$ m^{-1}/Chla (μg l^{-1})

[a] a_{CDOM} measured at 380 nm

$a_{CDOM(440)}$ (Amazon 4 = 5.9 m^{-1}). Further, dissolved organic matter derived from the fringing floodplain, i.e., allochthonous sources from leaching of forest litter and aquatic vegetation, also contributes to higher CDOM levels during receding waters (McClain & Elsenbeer, 2001). At rising water stage, the lower $a_{CDOM(440)}$ in the Amazon River is a result of a lower load of dissolved organic matter and lower discharge of the main tributaries: Negro, Madeira, and Solimões (Moreira-Turcq et al., 2003). For instance, at Amazon 1 station we measured lower $a_{CDOM(440)}$ (3.6 m^{-1}) at rising water compared with receding waters (10.6 m^{-1}) due to lower discharge of high CDOM waters of the Negro River at that phase of the hydrological cycle (Fig. 1). At the last Amazon station (Amazon 4), downriver from the confluence with the Tapajós River, $a_{CDOM(440)}$ values decreased to approximately 2.6 m^{-1}. Further, contributions from allochthonous sources from vegetated flooded areas are decreased at this period compared with the receding water stage when large dissolved organic matter contributions are expected (McClain & Elsenbeer, 2001).

In the sediment-laden waters, the measured high attenuation due to scattering by inorganic particulates and absorption by dissolved organic matter limits PAR to depths shallower than 1.0 m, and consequently prevents high productivity (here indicated as low levels of Chla ~ 0.3–0.5 μg l^{-1}) and lower phytoplankton community diversity. Table 3 shows lower concentration of pigments—most below the detection limit—in these sediment-laden waters. The low autochthonous primary production in these Amazonian rivers is well documented in terms of low chlorophyll concentrations and productivity (Fisher, 1979; Putz & Junk, 1997; Melack & Forsberg, 2001). According to our biomarker pigment results, the low productivity is represented by Cyanophyceae and Bacillariophyceae (in agreement with recent species composition data for the Amazon from Casali et al. (2012)), which are known to be adapted to low light conditions (Dokulil & Teubner, 2000). Diatoms, specifically, tend to show an increase in the concentration of the light harvesting fucoxanthin pigment in low light conditions (Descy et al., 2009). At the sampling phases of the hydrological cycle, water mixing allows phytoplankton to be exposed to spectral light available at the shallow euphotic depth. However, given the depth of the water mixing (often close to the bottom of the rivers, Dustan, 2009) and the

shallow euphotic depth (Table 1), the phytoplankton is only exposed to this light for a very short time (Fisher, 1979; Dustan, 2009), consequently the rate of photosynthesis in the water column decreases (Kirk, 1994). Light can possibly still be detected below $Z_{1\%}$ due to the diffuse nature of the angular distribution of the light field in scattering dominated waters, which results in strong contribution of upward scattered light to the total irradiance (Kirk, 1994; Bergmann et al., 2004). However, in these waters we also have to consider that light is not only highly scattered, but also absorbed by CDOM (Table 4 for correlations). This implies that at the same time when light is scattered, thus making it more available for phytoplankton absorption with little competition for photons, it is also more available to be absorbed by CDOM, thus making it less available for phytoplankton due to competition for short blue wavelength radiation (Kirk, 1994). Total light availability for phytoplankton can only be attested to by measuring underwater scalar irradiance with depth, which is shown to be quite different from planar irradiance, especially at shallow depths (Arst et al., 2008).

Sampled rivers with low TSS (Negro, Uatumã, Trombetas, and Tapajós) were generally characterized by lower and more variable K_d values compared with the high TSS rivers. Statistically, $a_{CDOM(440)}$ was the primary light attenuator in these waters (Table 4). However, the low number of samples representing a large range of, for instance, Chla concentrations, likely diminished the importance of this variable in the light attenuation process. Consequently, K_d variability among these rivers is likely a result of either $a_{CDOM(440)}$, Chla, or a combination of both. In the Negro River, for instance, with the highest CDOM and low Chla, light is mostly absorbed by CDOM. Concentrations of dissolved organic matter in this river are known to be very high (Moreira-Turcq et al., 2003) as a result of the characteristics of the river's drainage basin, which is covered by inundated forest on the Guyana Shield and the lowlands, and highly weathered lateritic and shallow podsol soils. This combination of inundated forest and soils allows for quick percolation of rain, resulting in large quantities of dissolved organic matter transported to the river. The high magnitude of dissolved organic matter depletes the light field of blue and green light at very shallow depths. As a result, the available irradiance is marked by red light (690 nm—Fig. 3). At the depth of half of $Z_{1\%}$, we measured 166.7 μmol m^{-2} s^{-1} of quantum irradiance at receding waters, similar to the value measured in the Uatumã River, and approximately twice the quantum irradiance measured in high TSS rivers (Fig. 4). In these highly absorbing waters, inhibition of photosynthesis due to competition for shortwave photons is likely happening, and photosynthetic activity relies mostly on absorption of available red light. The phytoplankton groups (Dinophyceae, Cyanophyceae, and Bacillariophyceae—similar to Fisher, 1979; Putz & Junk, 1997; Saliot et al., 2001) indicated by the biomarker pigments are probably using different strategies to photosynthesize in a low light environment and narrowed to red light. For instance, Dinophyceae and Bacillariophyceae are adapted to low light conditions, and the biliprotein pigments found in Cyanophyceae absorb strongly in the red part of the spectra (Kirk, 1994), yet productivity in these waters is considerably low, as indicated by the Chla level (<2.0 μg l^{-1}).

Seasonally, the Uatumã River exhibited a different spectral irradiance profile at rising waters when compared with receding waters (Fig. 3). At the rising water stage, $E'_{d(\lambda)}$ shows three wavelength maximums (585, 650, and 690 nm), and minimums at 620 and 670 nm, similar to the Trombetas and Tapajós Rivers (Fig. 3c, d). The $E'_{d(\lambda)}$ minimums are possibly a result of light absorption by phycocyanin in Cyanophyceae, which was one of the planktonic group indicated by our biomarker pigment analysis, and have often been reported during this season, especially in the Tapajós River (Putz & Junk, 1997; Sa et al., 2010). In the Tapajós River, an increase in algal abundance (Chla ~ 18.3 μg l^{-1}) resulted in higher light absorption and scattering, and consequently higher K_{ds} (K_{d_B} ~ 3.0 m^{-1}, K_{d_G} ~ 1.9 m^{-1}, and K_{d_B} ~ 1.7 m^{-1}), lower quantum irradiance at the depth of half $Z_{1\%}$ (80.5 μmol m^{-2} s^{-1}), and lower $Z_{1\%}$ (2.6 m) compared with the Trombetas River (K_{d_B} ~ 2.0 m^{-1}, K_{d_G} ~ 1.2 m^{-1}, and K_{d_B} ~ 1.1 m^{-1}; q_{dPAR} ~ 159.3 μmol m^{-2} s^{-1}, and $Z_{1\%}$ ~ 4.1 m) and Uatumã River (K_{d_B} ~ 2.4 m^{-1}, K_{d_G} ~ 1.4 m^{-1}, and K_{d_B} ~ 1.0 m^{-1}; q_{dPAR} ~ 189.9 μmol m^{-2} s^{-1}, and $Z_{1\%}$ ~ 3.8 m). Blooms of Chla in the Tapajós waters have been reported at the rising water stage, and are suggested to be associated with increased cattle ranching in the floodplain regions (Novo et al., 2006). However, the relationship

between cattle ranching and concentrations of Chla needs to be further investigated to be confirmed.

At receding waters, contrasting results from the Negro and Uatumã Rivers, the light climate in the Tapajós and Trombeta Rivers was characterized by the highest $Z_{1\%}$, the lowest K_d values, and consequently the highest quantum irradiance at the depth of half $Z_{1\%}$ (220.0 μmol m^{-2} s^{-1}). While both rivers exhibited similar quantum irradiance at the depth of half $Z_{1\%}$, the spectral characteristics of the light field were different. In the Tapajós River, irradiance was mostly dominated by green (580 nm) and red (650–700 nm) light (Fig. 3b); while in the Trombetas River, light was marked by a defined peak at around 690 nm (Fig. 3b). These differences are likely more related to water mixing of the Trombetas River with the Amazon River than with differences in the sub-basin characteristics and biogeochemical processes. Both the Trombetas and Tapajós Rivers are classically characterized by low TSS and DOM due to the similarities of their headwaters in Precambrian shields (Devol & Hedges, 2001; Moreira-Turcq et al., 2003). However, at receding waters, measured concentrations of TSS and $a_{CDOM(440)}$ in the Trombetas were about twice those of the Tapajós waters, which could be a result of mixing with Amazon waters flowing through the intricate floodplain into the Trombetas River. Similar optical mixing has been reported by studies of the spectral reflectance of other Amazonian waters (Rudorff et al., 2009). The increased concentrations of CDOM in the Trombetas waters lead to higher absorption in the blue and green spectra, therefore, increasing K_{d_B} (3.0 m^{-1}) and K_{d_G} (2.0 m^{-1}) (Fig. 4a), and higher scattering in all wavelengths, thus skewing the irradiance at $Z_{1\%}$ to red light (690 nm), similar to that of the high sediment waters (Fig. 3b). In the Tapajós waters, however, the higher Chla and low $a_{CDOM(440)}$ resulted in the lowest K_d ($K_{d\_B} \sim 1.3$ m^{-1}, $K_{d\_G} \sim 0.8$ m^{-1}, and $K_{d\_B} \sim 0.7$ m^{-1}) of all sampled rivers at receding waters. Accordingly, irradiance at $Z_{1\%}$ was spectrally depleted of blue light due to phytoplankton and CDOM absorption and dominated by green and red light, with marked minimums at 620 and 670 nm due to Cyanophyceae pigment absorption.

We have shown the differences in the light field of large Amazonian rivers as a function of the quantity and quality of their optically active water constituents. How the light condition might change as a consequence of, for example, resource extraction in the Amazon can be demonstrated with the data presented here. For instance, numerous small-scale gold mining activities in the watershed of the Tapajós River since the 1950s have resulted in high concentrations of very fine grain latosol sediment being injected into this river from different tributaries. One of these tributaries is the heavily mined Creporí River, which originally had waters as clear as the Tapajós River and currently shows TSS of up to 500 mg l^{-1}. Concentrations of suspended solids in the Tapajós River upstream of the confluence of Creporí River are about 7 mg l^{-1}, and concentrations are higher than 100 mg l^{-1} downstream of the confluence (Telmer et al., 2006). We can speculate that the light field of the affected tributaries and vast areas of the Tapajós River have changed, with a considerable increase in light scattering due to a higher concentration of suspended solids resulting in a decrease in the quantity of light at any depth and a shift from a green/red to a red dominated light field in a narrower euphotic layer. These changes are likely causing a decrease in photosynthetic activity, and are almost certainly leading to shifts in biological communities. Although we have not yet quantified the light field changes in waters under the influence of mining activities, it surely occurs, as has been shown by studies reporting decreases in phytoplankton (Guenther & Bozelli, 2004a) and fish diversity (Mol & Ouboter, 2003) in other affected waters in the Amazon.

Other types of land-use change occurring in the Amazon basin, such as the conversion of forest and floodplain into pastureland or soy plantations (Thomas et al., 2004) and hydroelectric power plants (present, under construction, and planned) (Melack & Forsberg, 2001; Leite et al., 2011), must also affect the light field in drainage waters, albeit the dynamics may be different due to different seasonal and physical forcings. We are not aware of any research investigating this problem; however, it has been shown that streams affected by land-use change do experience increases in particulate matter (Thomas et al., 2004). Given the estimated deforestation rates in the Amazon forest of 19,000 km^2 $year^{-1}$ from 1997 to 2003 (INPE, 2004), and deforestation of the floodplain, 56% from 1975 to 2008 (Renó, 2010), changes in the inputs to the rivers are undoubtedly already occurring, and these must be driving changes in the water light field.

Summary and conclusion

Changes in both quality and quantity of in-water light occur as a result of the variability of the water optical constituents and the incoming light (Kirk, 1994). By constraining the incoming light conditions—our data was acquired at narrow solar elevation range and close to the equator—we have shown the variability of the spectral light field and associated optical water constituents in large rivers of the Amazon Basin, at receding and rising water stages. We recognize that this is a spatially and temporally limited dataset, sampling on seven large rivers and at only two stages of the hydrological cycle. We also acknowledge optical instrument limitations to perform accurate measurements of short wavelength light (<450 nm) in highly attenuated waters. Nonetheless, the presented data provides the first investigation of the underwater spectral light field and associated biogeochemical variables in the Amazon main rivers. Our results have demonstrated that the underwater spectral light field is distinctly different among the Amazonian rivers and between the two sampled water stages as a result of the variability of the water optical constituents, which in turn are linked to the sources, physical processes, and biogeochemical reactions in the rivers' sub-basin, hydrology, and water mixing between rivers.

High concentrations of suspended matter of inorganic nature and CDOM in rivers with headwaters in the Andean Cordillera (Amazon, Solimões, and Madeira) significantly affected the diffuse attenuation coefficient due to non-selective light scattering and blue/green light absorption. In the well-mixed shallow euphotic water column, the light field was mostly confined to red light, for both receding and rising water stages. The noteworthy difference between the two sampling periods was mostly related to higher magnitudes of spectral attenuation coefficients at rising water stage due to much higher concentrations of suspended matter in the water and, as a result, light diminished to the lowest levels and was limited to shallower depths. Light restriction in these waters limits primary production and phytoplankton community diversity to low levels, as expressed by the low Chla concentrations and pigment analysis, respectively. This may account for the presence of Cyanophyceae, which have low light requirements and contain photosynthetic pigments to take advantage of available red light.

Rivers with headwaters in the Guyana (Negro, Uatumã, and Trombetas) and Brazilian (Tapajós) shields generally exhibited the lowest concentrations of suspended matter among all the sampled rivers. Noticeable biogeochemical variability among these rivers included year-round high CDOM in the Negro River, lower CDOM in the Uatumã and Trombetas at rising waters, and higher Chla in the Uatumã, Trombetas, and especially in the Tapajós River at rising waters compared with receding waters. In these low TSS waters, absorption by CDOM significantly defined the attenuation of blue and green light. However, the low number of samples representing a larger range of Chla concentrations may have contributed to the diminished role of phytoplankton as light attenuator. For instance, the role of phytoplankton as light attenuator was noticeable in the irradiance curves of the Uatumã and Tapajós Rivers at rising water stage when Chla concentrations were the highest. The light field in these rivers exhibited less absorption of green light when compared with the Negro River, and also marked minimums at 620 and 670 nm as a result of light absorption by phycocyanin in Cyanophyceae, a planktonic group indicated in the biomarker pigment analysis. While the spectral curves of both rivers were similar, the total PAR irradiance at the depth of $Z_{1\%}$ was about half in the Tapajós compared with the Uatumã River as a result of higher light absorption by Chla in the former. The effect of CDOM absorption on the light field was mostly notable at the receding waters of the Negro, Uatumã, and Trombetas Rivers, when the light field was spectrally confined to red wavelengths as the blue and green wavelengths were selectively absorbed, resulting in irradiance curves similar to the rivers with headwaters in the Andean Cordillera. However, fewer scattering processes due to lower TSS allowed light to define a deeper $Z_{1\%}$. In these waters, inhibition of photosynthesis due to competition for short wavelength light is likely happening, and planktonic groups such as Dinophyceae and Bacillariophyceae prevail because of adaptation to low light conditions.

Land-use change in the Amazon, for instance, forest and floodplain conversion into pasture and farmland, mineral resources extraction, and hydroelectric construction can potentially influence the in-water light condition in the Amazonian rivers. We hope that by presenting this dataset of the light field in large Amazonian rivers, we are providing a valuable

contribution for better understanding the ecology and biogeochemistry of Amazonian rivers, and that consequently the effects of human disturbances can be better monitored and managed to minimize ecological damage.

Acknowledgments We wish to thank the National Science and Engineering Research Council of Canada (NSERC), the Brazilian National Institute of Space Research (Instituto Nacional de Pesquisas Espaciais-INPE), the Fundação de Amparo a Pesquisa do Estado de São Paulo (FAPESP grant no. 2004/12495-5 and FAPESP grant no. 2004/14086-5 to Costa and Telmer), and the University of Victoria for financial support; Dr. Bernardino Figueiredo for facilitating collaboration with FAPESP, Ricardo Rossin for assistance with analytical geochemistry, and Conrado Rudorff and Dr. Waterloo P. Filho for fieldwork assistance. The authors also thank the anonymous reviewers for the valuable suggestions which significantly improved the scientific quality of this manuscript.

References

APHA, 1998. Standard Methods for the Examination of Water and Wastewater. APHA, Washington, DC.

Arst, H., A. Reinart & M. Hussainov, 2000. Influence of the depth-dependence of the PAR diffuse attenuation coefficient on the computation of downward irradiance in different water bodies. Geophysica 36: 129–139.

Arst, H., T. Noges, P. Noges & B. Paavel, 2008. Relations of phytoplankton in situ primary production, chlorophyll concentration and underwater irradiance in turbid lakes. Hydrobiologia 599: 169–176.

Bergmann, T., G. L. Fahnenstie, S. Lohrenz, D. Milliem & O. Schofield, 2004. Impacts of a recurrent resuspension event and variable phytoplankton community composition on remote sensing reflectance. Journal of Geophysical Research 109: 1–12.

Boss, E., L. Tylor, S. Gilbert, K. Gunderson, N. Hawley, C. Janzen, T. Johengen, H. Purcell, C. Robertson, D. W. H. Schar, G. J. Smith & M. N. Tamburii, 2009. Comparison of inherent optical properties as a surrogate for particulate matter concentration in coastal waters. Limnology and Oceanography: Method 7: 803–810.

Bozelli, R. L. & A. V. Garrido, 2000. Gradient of inorganic turbidity and responses to planktonic communities in an Amazonian lake, Brazil. Verhandlungen der Internationale Vereinigung für Limnologie 27: 147–151.

Casali, S., M. C. Calijuri, B. Barbarisi, V. F. Reno, A. G. Affonso, C. Barbosa, T. S. F. Silva & E. M. L. M. Novo, 2012. Impact of the 2009 extreme water level variation on phytoplankton community structure in lower Amazon floodplain lakes. Acta Limnologica Brasiliense 23: 260–270.

Descy, J. P., H. Sarmento & H. W. Higgins, 2009. Variability of phytoplankton pigment ratio across aquatic environments. European Journal of Phycology 44: 319–330.

Devol, A. H. & J. I. Hedges, 2001. Organic matter and nutrients in the mainstem Amazon River. In McClain, M. E., R. L. Victoria & J. E. Richey (eds), The Biogeochemistry of the Amazon Basin. Oxford University Press, Oxford: 275–306.

Dokulil, M. T. & K. Teubner, 2000. Cyanobacterial dominance in lakes. Hydrobiologia 438: 1–12.

Dunne, T., L. A. K. Mertes, R. H. Meade, J. E. Richey & B. R. Forsberg, 1998. Exchanges of sediment between the flood plain and channel of the Amazon River in Brazil. Geological Society of America Bulletin 110: 450–467.

Dustan, P., 2009. Terrestrial limitations of Amazon River productivity: why the Amazon River is not green. Evolutionary Ecology Research 11: 421–432.

EPA, 1997. Method 447.0. Determination of chlorophyll *a* and *b* and identification of other pigments of interest in marine and freshwater algae using high performance liquid chromatography with visible wavelength detection: 20 pp.

Ertel, J. R., J. I. Hedges, A. H. Devol, J. E. Richey & M. N. Goes Ribeiro, 1986. Dissolved humic substances of the Amazon River System. Limnology and Oceanography 31: 739–754.

Fisher, T. R., 1979. Plankton and primary production in aquatic systems of the Central Amazon Basin. Comparative Biochemistry Physiology 62A: 31–38.

Forsberg, B. F., A. H. Devol, J. E. Richey, L. Martinelli & U. dos Santos, 1988. Factors controlling nutrient distributions in Amazon lakes. Limnology and Oceanography 33: 41–56.

Furch, B., A. F. F. Corrêa, J. A. S. Nunes de Mello & K. R. Otto, 1985. Light regimes in three aquatic ecosystems of different physico-chemical properties. I. Attenuation, irradiance reflectance and comparison between downwelling, upwelling and scalar irradiances (PAR). Amazoniana 3: 411–430.

Guenther, M. & R. Bozelli, 2004a. Effects of inorganic turbidity on the phytoplankton of an Amazonian Lake impacted by bauxite tailings. Hydrobiologia 511: 151–159.

Guenther, M. & R. Bozelli, 2004b. Factors influencing algae-clay aggregation. Hydrobiologia 523: 217–223.

INPE, 2004. Monitoramento da Floresta Amazonica Brasileira por Satélite. Projeto PRODES.

Irion, G., W. J. Junk & J. A. S. Nunes de Mello, 1997. The large Central Amazon river floodplains near Manaus: geological, climatological, hydrological, and geomorphological aspects. In Junk, W. J. (ed.), The Central Amazon Floodplain: Ecology of a Pulsing System. Springer-Verlag, Berlin: 23–46.

Junk, W. J. & H. J. Krambeck, 2000. Climate and hydrology. In Junk, W. J., J. J. Ohly, M. T. F. Piedade & M. G. M. Soares (eds), The Central Amazonian Floodplain: Actual Use and Options for a Sustainable Management. Backhuys Publisher, Leiden, The Netherlands: 95–108.

Kauer, T., H. Arst & L. Tuvikene, 2010. Underwater light field and spectral distribution of attenuation depth in inland and coastal waters. Oceanologia 52: 155–170.

Kirk, J. T. O., 1994. Light and Photosynthesis in Aquatic Systems. Cambridge University Press, New York.

Kirk, J. T. O., 2003. The vertical attenuation of irradiance as a function of the optical properties of the water. Limnology and Oceanography 48: 9–17.

Konhauser, K. O., W. S. Fyfe & Kronberg, B. I., 1994. Multielement chemistry of some Amazonian waters and soils. Chemical Geology 111: 155–175.

Leite, N. K., A. V. Krusche, M. V. R. Ballester, R. L. Victoria, J. E. Richey & B. M. Gomes, 2011. Intra and interannual

variability in the Madeira River water chemistry and sediment load. Biogeochemistry 105: 37–51.

Loisel, H., X. Mériaux, J. F. Berthon & A. Poteau, 2007. Investigation of the optical backscattering to scattering ratio of marine particles in relation to their biogeochemical composition in the eastern English Channel and southern North Sea. Limnology and Oceanography 52: 739–752.

Mantoura, R. F. C. & D. J. Repeta, 1997. Calibration methods for HPLC. In Jeffrey, S. W., R. F. C. Mantoura & S. W. Wright (eds), Phytoplankton Pigments in Oceanography: Guidelines to Modern Methods. SCOR-UNESCO, Paris: 407–428.

Marengo, J. A., J. Tomasella, L. M. Alves, W. R. Soares & D. A. Rodriguez, 2011. The drought of 2010 in the context of historical droughts in the Amazon region. Geophysical Research Letters 38: L12703.

McClain, M. E. & H. Elsenbeer, 2001. Terrestrial inputs to Amazon streams and internal biogeochemical processing. In McClain, M., E. R. L. Victoria & J. E. Richey (eds), The Biogeochemistry of the Amazon Basin. Oxford University Press, Oxford: 185–208.

McClain, M. E., J. E. Richey & J. A. Brandes, 1997. Dissolved organic matter and terrestrial-lotic linkages in the central Amazon basin of Brazil. Global Biogeochemical Cycles 11: 295–311.

Meade, R. H., 1994. Suspended sediments of the modern Amazon and Orinoco rivers. Quaternary International 21: 29–39.

Meade, R. H., 2007. Transcontinental moving and storage: the Orinoco and amazon rivers transfer the Andes to the Atlantic. In Gupta, A. (ed.), Large Rivers: Geomorphology and Management. Wiley, Chichester: 45–63.

Melack, J. M. & B. R. Forsberg, 2001. Biogeochemistry of Amazon floodplain lakes and associated wetlands. In McClain, M. E., R. L. Victoria & J. E. Richey (eds), The Biogeochemistry of the Amazon Basin. Oxford University Press, Oxford: 125–274.

Mol, J. H. & P. E. Ouboter, 2003. Downstream effects of erosion from small-scale gold mining on the instream habitat and fish community of a small neotropical rainforest stream. Conservation Biology 18: 201–214.

Moreira-Turcq, P., P. Seyler, J. L. Guyot & H. Etcheber, 2003. Export of organic carbon from the Amazon River and its main tributaries. Hydrological Processes 17: 1329–1344.

Novo, E. M. L. M., C. C. F. Barbosa, R. M. de Freitas, Y. E. Shimabukuro, J. M. Melack & W. Pereira Filho, 2006. Seasonal changes in chlorophyll distributions in the Amazon floodplain lakes derived from MODIS images. Limnology 7: 153–161.

Paavel, B., H. Arst, A. Reinart & A. Herveli, 2006. Model calculations of diffuse attenuation coefficient spectra in lake waters. Proceedings of the Estonian Academy of Sciences: Biology, Ecology 55: 61–81.

Putz, R. & W. J. Junk, 1997. Phytoplankton and Periphyton. In Junk, W. J. (ed.), The Central Amazon Floodlpain: Ecology of a Pulsing System. Springer-Verlag, Berlin: 147–181.

Reinart, A. & H. Arst, 1998. Relation between underwater irradiance and quantum irradiance in dependence on water transparency at different depths in the water bodies. Journal of Geophysical Research 103: 7749–7752.

Reinart, A. & A. Herlevi, 1996. Diffuse attenuation coefficient in some Estonian and Finnish lakes. Proceedings of the Estonian Academy of Sciences Biology Ecology 48: 267–283.

Reinart, A., B. Paavel & L. Tuvikene, 2004. Effect of coloured dissolved organic matter on the attenuation of photosynthetically active radiation in Lake Peipsi. Proceedings of the Estonian Academy of Sciences Biology Ecology 53: 88–105.

Renó, V. F., 2010. Deforestation assessment on the lower Amazon floodplain using Landsat images observation from 1975 to 2008. MSc Thesis, Brazilian Institute for Space Research, São Paulo.

Richey, J. E., R. H. Meade, E. Salati, A. H. Devol, C. F. Nordin & U. Santos, 1986. Water discharge and suspended sediment concentrations in the Amazon River: 1982–1984. Water Resources Researcher 22: 756–764.

Roland, F. & F. A. Esteves, 1998. Effects of bauxite tailing on PAR attenuation in an Amazonian crystalline water lake. Hydrobiologia 377: 1–7.

Rudorff, C. M., L. S. Galvao & E. M. L. M. Novo, 2009. Reflectance of floodplain water bodies using EO-1 Hyperion data from high and receding flood periods of the Amazon River. Remote Sensing of Environment 30: 2713–2720.

Sa, L. L. C., J. M. S. Vieira, R. A. Mendes, S. C. C. Pinheiro, E. R. Vale, F. A. S. Alves, I. M. Jesus, E. C. O. Santos & V. B. Costa, 2010. Occurrence of toxic cyanobacterial bloom in the left margin of the Tapajos River, in the municipality of Santarem (Para State, Brazil). Revista Pan-Amazon Saude 1: 159–166.

Saliot, A., L. Mejanelle, P. Scribe, J. Fillaux, C. Pepe, A. Jaboud & J. Dagout, 2001. Particulate organic carbon, sterols, fatty acids and pigments in the Amazon River system. Biogeochemistry 53: 70–103.

Squires, M. M. & F. W. L. Lesack, 2003. Spatial and temporal patterns of light attenuation among lakes of the Mackenzie Delta. Freshwater Biology 43: 1–20.

Sun, D., Y. Li, Q. Wang, J. Gao, H. Lv, C. Le & C. Huang, 2009. Light scattering properties and their relation to the biochemical composition of turbid productive waters: a case study of Lake Taihu. Applied Optics 48: 1979–1989.

Telmer, K., M. P. F. Costa, R. S. Angélica, E. S. Araujo & Y. Maurice, 2006. The source and fate of sediment and mercury in the Tapajos River, Para, Brazilian Amazon: ground- and space-based evidence. Journal of Environmental Management 81: 101–113.

Thomas, S. M., C. Neill, L. A. Deegan, A. V. Krusche, V. M. Ballester & R. L. Victoria, 2004. Influences of land use and stream size on particulate and dissolved materials in a small Amazonian stream network. Biogeochemistry 68: 135–151.

Tudesque, L., G. Grenouillet, M. Gevrey, K. Khazraie & S. Brosse, 2012. Influence of small-scale gold mining on French Guiana streams: are diatom assemblages valid disturbance sensors? Ecological Indicators 14: 100–106.

Walker, I., 1990. Ecologia e biologia dos igapós e iagarpés. Ciência Hoje 11: 44–53.

Wright, S. W. & S. W. Jeffrey, 2006. Pigment markers for phytoplankton production. In Volkman, J. K. (ed.), Marine Organic Matter: Biomarkers, Isotopes and DNA. The Handbook of Environmental Chemistry, Vol. 2, Part 2N. Springer-Verlag, Basel: 71–104.